Proceedings of the 9th JFPS International Symposium on Fluid Power, Matsue, 2014
Oct. 28 - 31, 2014

S-3

STUDY ON COMPRESSED AIR ENGINE

Cai Maolin, Yu Qihui

School of Automation Science and Electrical Engineering
Beihang University
Beijing, 100191 China
(E-mail: caimaolin@buaa.edu.cn)

ABSTRACT

As a kind of zero pollution power media, compressed air can be used to drive a car engine. Instead of the internal combustion engines, the compressed air engine (CAE) equipped on an automobile can transform the energy of compressed air into the mechanical energy. To establish a foundation for the optimization of the CAE, a dimensionless mathematical model is set up. The dimensionless energy efficiency and output power characteristics of the CAE can be found. To prevent the ice blocking problem during the engine's operation, temperature drops at critical positions are analyzed and a heat exchange system is designed. It can be concluded, firstly, the dimensionless efficiency is influenced significantly by the dimensionless exhaust pressure, the intake duration angle, and the exhaust duration angle. Secondly, the dimensionless power is affected significantly by the scale factor of the exhaust valve, the intake duration angle, the dimensionless exhaust pressure and the dimensionless inertial moment parameter. Third, the optimal output power and efficiency values are 2.027kW and 50.13%, respectively. Moreover, simulation results show that the heat exchange system can maintain the air temperatures in the supply system above 0℃. Lastly, the mathematical model is verified experimentally. This research can be a theoretical support in the design and optimization of the CAE.

KEYWORDS

Compressed air engines, Energy efficiency, Output power, Dimensionless mathematical model, Heat exchange system

NOMENCLATURE

- A_p: piston area (m^2)
- A_h: heat transfer area (m^2)
- A_{emax}: the maximum effective cross-sectional area (m^2)
- c_1, c_2: coefficients
- CVL: exhaust valve lift (mm)
- D: cylinder bore diameter (m)
- E: available energy of compressed air (J)
- G: air mass flow (kg/s)
- IVL: intake valve lift (mm)
- J: the moment of inertia of crankshaft, flywheel, main gear and rotating part of connecting rod (kg.m^2)
- κ: specific heat ratio (=1.4)
- L: connecting rod length (m)
- m: air mass(kg)
- M: piston, rings, pin and small end of connecting rod mass (kg)
- n: rotate speed (rpm)
- p: pressure
- r: crank radius (m)
- R: gas constant
- S: stroke (m)
- t: time (s)
- T_L: load torque (N.m)
- T_r: reciprocating torque (N.m)
- W: output work (J)
- β: connecting rod angle (rad)
- τ_1, τ_2: scale factor of intake valve and exhaust valve

θ: crankshaft angular position (rad)
η: efficiency
λ: the ratio of crank radius and connecting rod length
T_i: indicated torque (N.m)
ω: angle speed (rad/s)

Subscripts
1: intake
2: exhaust
a: atmospheric
d: downstream side
u: upstream side
s: supply

Superscript
*: Dimensionless

INTRODUCTION

Pressure has been growing over decades on the issues of environmental pollution and energy crisis. It is estimated that oil and gas reserves can last until 2042[1]. Consequently, the use of unconventional energy sources has been widely concerned. It is anticipated by 2100, renewable energy may account for 20-30% of the world energy consumption [2]. The internal combustion engines (ICE) not only consume large amounts of oil but also lead to serious environmental pollutions. So the ICE technology must be improved. Three types of zero emission engine technologies have been proposed and investigated extensively over the past two decades, hydrogen engines [3-6], electric engines [7-8] and compressed air engines [9-11]. Hydrogen engines and electric engines are still releasing pollutants into the air. For the conception of green energies, this paper is concerned with engine using compressed air.

The CAE converts the energy of compressed air into the mechanical energy. Compared to the electrical motor, the CAE is safer, cleaner, cheaper and has higher power-to-weight ratio [12-13]. As a form of storage, compressed air is nothing new. Indeed, the CAE has been utilized in power mining locomotives in the United States and Europe at the beginning of the 20th century [14]. Figure (1) shows the early compressed air vehicle.

Figure1. Some early compressed air vehicle

During past decades, many company focus on CAE. MDI, a French company of air powered vehicles developed a series of CAEs. The CAE from MDI is a significant step for zero-emission transport, delivering a compressed air-driven vehicle that is safe, quiet, has a top speed of 110km/h and a range of 200km. The Figure (2) shows CAE and compressed air vehicle from MDI. Engineair Pty Ltd, is another company focusing on the development of air motor technology based on a unique rotary piston concept. The air motor and vehicle are shown in Figure (3) [15].

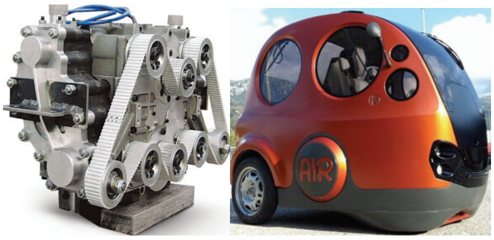

Figure2. CAE and compressed air vehicle from MDI

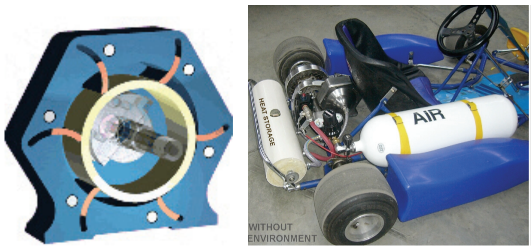

Figure3. CAE and compressed air vehicle from Engineair company

Besides company, many researches focused on improving the efficiency of the CAE [16-18]. But most of these studies only improved specific parameters or calculated overall efficiency, thus the results are not suitable for optimizing the complex CAE system. And besides the efficiency, the output power and the temperature are also important factors in the application of a CAE. But only a few studies have focused on these issues [19]. In China, some universities and companies have also been conducting researches and designs on kinds of CAEs [20-22]. Generally limited by problems of low working efficiency and low temperature, the CAE is still in developing stage. Low temperature due to the air's expansion and the local throttling can lead to poorer power performance of the compressed air, and can even result in ice blockings at critical locations of the CAE system which is a problem cannot be ignored. Liu Hao and Chih Yung Huang both mentioned that there was a certain temperature decrease in the cylinder of the CAE and higher inlet pressures resulted in lower temperatures [23]. Zhai Xin reported that increasing the inlet temperature is an effective way to enhance the engine's power and efficiency, and Zhai also studied the optimization of the CAE's inlet tube for the best heat transfer performance [16]. Few studies established complete heat transfer models of the CAE system, as well as methods to calculate the air temperature drops at critical locations, especially the high pressure reducing valve and the exhaust port of the CAE.

Several studies provided references for the temperature analysis of the compressed air system. The Joule-Thomson coefficient was used to calculate the temperature changes of the throttling. The real gas effect on temperature was considered in the discharging process of high pressure vessels. But most of these methods need to solve transcendental equations which have large calculation complexity, thus they are not suitable for modeling of dynamic pneumatic systems.

This paper focuses on the multi-objective optimization of the CAE system. For the optimization of the CAE system, a dimensionless model of the system is established by selecting appropriate reference values. Then, the analysis and optimization of parameters are performed. To prevent the ice blocking problem, a heat transfer system is designed. Results of this paper are helpful to improve the performance of the CAE system.

WORKING PRINCIPLE OF THE CAE

For a piston-type CAE, the compressed air expands in the cylinder, pushing the piston to output shaft power. Its operation is shown in Figure (3): in the suction power stroke the compressed air enters the cylinder through the intake valve, driving the piston downward. Then the intake valve closes after a specific crank angle while the compressed air expands to push the piston down and output work. When the piston is near the bottom dead center the exhaust valve opens so that the air with residual pressure discharges under the impetus of the piston. After the piston moves back to the top dead center, the CAE completes a work cycle.

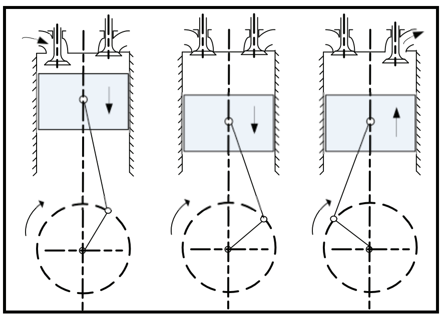

Figure3. Working cycle of the CAE

DIMENSIONLESS MATHMATICAL MODELS

Dynamic model of the CAE

The basic thermodynamic mathematical model can be referenced in the author's previous work [24]. Figure (4) shows a model of a CAE coupled to a load. The following equation, derived from Newton's principle for a rotation body describes the dynamics of the system.

$$T_i - T_r - T_L = J\ddot{\theta} \tag{1}$$

The indicated torque (T_i) is generated by the conversion of compressed air energy to mechanical energy during the working process. The reciprocating torque (T_r) is produced by the motion of the piston assembly and the small end of the connecting rod. T_L is load torque; J is the moment of inertia of crankshaft, flywheel, main gear and rotating part of connecting rod.

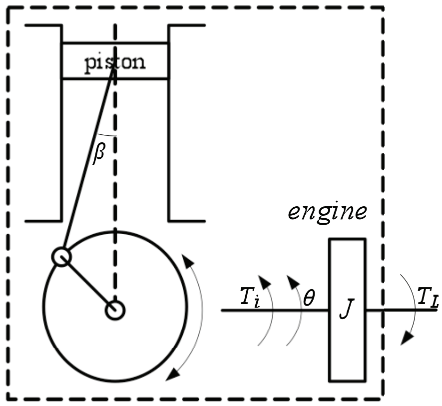

Figure 4 Engine and load model

The relationship between the pressure inside cylinder (p), and the indicated torque (T_i), can be expressed as

$$T_i = pArG(\theta) \tag{2}$$

where

$$G(\theta) = \frac{\sin(\theta + \beta)}{\cos\beta} \tag{3}$$

β can be expressed as

$$\beta = \sin^{-1}\frac{r\sin\theta}{L} \tag{4}$$

$$\lambda = r/L \tag{5}$$

From the piston-crank geometry, the piston displacement (y) can be given by

$$y = r + L - r\cos\theta - L\cos\beta \tag{6}$$

The cylinder volume can be given by

$$V(\theta) = \frac{\pi D^2 y}{4} + V_c \tag{7}$$

The reciprocating torque (T_r), is given by

$$T_r = -m_r r \omega^2 G_1(\theta) - m_r r \dot{\omega} G_2(\theta) \tag{8}$$

where

$$G_1(\theta) = \cos\theta + \frac{\lambda\cos 2\theta}{\left(1-\lambda^2\sin^2\theta\right)^{1/2}} + \frac{\lambda^3\sin^2 2\theta}{4\left(1-\lambda^2\sin^2\theta\right)^{3/2}} \tag{9}$$

$$G_2(\theta) = \sin\theta + \frac{\lambda\sin 2\theta}{2\left(1-\lambda^2\sin^2\theta\right)^{1/2}} \tag{10}$$

For the convenience of analysis, the load torque is given by

$$T_L = c_1 + c_2\dot{\theta} \tag{11}$$

The effective sectional area of the intake and exhaust valve can be expressed as

$$A_1 = \begin{cases} A_{1\max} & 0 \le \theta < \theta_1 \\ 0 & \text{others} \end{cases} \tag{12}$$

$$A_2 = \begin{cases} A_{2\max} & \theta_2 \le \theta < 2\pi \\ 0 & \text{others} \end{cases} \tag{13}$$

The maximum effective cross-sectional area and piston area can be illustrated by Figure (5).

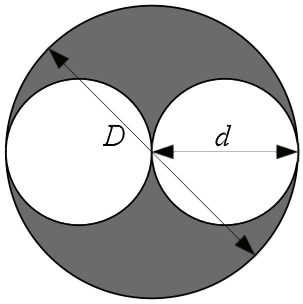

Figure 5. The relationship between the maximum effective cross sectional and piston area

According to Figure (5), the maximum effective area can be expressed as

$$A_{e\max} = \frac{\pi D^2}{16} \tag{14}$$

Dimensionless Model

To set a foundation for the study on optimization of CAE, further research on output power and efficiency characteristics are essential. CAE system is a complex system. Output power and efficiency are influenced by many parameters. Dimensionless mathematical model of the CAE is proposed to obtain key parameters. The reference values and the dimensionless variables are shown in Table (1). The basic mathematical can be made dimensionless as described in the following section.

Table1 Reference values and dimensionless variables

Variable	Reference value	Dimensionless variable
Displacement	S Stroke	$x^*=x/S$
Area of piston	A_p Area of piston	$A^*=A/A_p$
Volume	$V_b=A_p.S$	$V^*=V/V_b$
Pressure	p_s Supply pressure	$p^*=p/p_b$
Temperature	T_a Atmosphere temperature	$T^*=T/T_a$
Air mass flow	$G_b = G_{\max} = \frac{A_{e\max} p_s}{\sqrt{T_a}} \left(\frac{2}{\kappa+1}\right)^{\frac{1}{\kappa-1}} \sqrt{\frac{2\kappa}{R(\kappa+1)}}$ Maximum air mass flow	$G^*=G/G_{max}$
Air mass	$m_b = \frac{p_s V_b}{R T_a}$	$m^*=m/m_b$
Time	$t_b = \frac{m_b}{G_b}$	$t^*=t/t_b$

Work	$W_b = p_s V_b$	$W^*=W/W_b$
Power	$P_b = W_b / t_b$	$P^*=P/P_b$
Torque	$T_b = p_s V_b / 2M$	$T_{or}^*=T_{or}/T_b$
Speed	$\omega_b = 2M / t_b$	$\omega^*=\omega/\omega_b$

The dimensionless energy equation becomes

$$\frac{dT^*}{dt^*} = \frac{1}{m^*}\left[\frac{1}{t_{hc}^*}A_h^*\left(T_a^* - T^*\right) + \kappa G^* T_i^* - G^* T^* - (\kappa - 1)\, p^* \frac{dV^*}{dt^*}\right] \tag{15}$$

where, the dimensionless parameter t_{hc}^* , which is the dimensionless temperature settling time of the cylinder, is the ratio of the temperature settling time constant, t_{hc}, and the time reference value, t_b [25]. The dimensionless and dimensional time constant can be written as follows

$$t_{hc}^* = \frac{t_{hc}}{t_b} \tag{16}$$

$$t_{hc} = \frac{C_v m_b}{a A_b} \tag{17}$$

$$A_h^* = 2 + 4\frac{y^*}{D^*} \tag{18}$$

The dimensionless equation of continuity can be given as the following equation

$$\frac{dm^*}{dt^*} = G^* \tag{19}$$

The dimensionless flow equation becomes

$$G_i^* = \begin{cases} \Pi \dfrac{B}{\kappa} \dfrac{p_u^* a_d^*}{\sqrt{T_u^*}} \sqrt{\left(\dfrac{p_d^*}{p_u^*}\right)^{\frac{2}{\kappa}} - \left(\dfrac{p_d^*}{p_u^*}\right)^{\frac{\kappa+1}{\kappa}}} & \dfrac{p_d^*}{p_u^*} > 0.528 \\ \Pi \dfrac{p_u^* a_d^*}{\sqrt{T_u^*}} & \dfrac{p_d^*}{p_u^*} \leq 0.528 \end{cases} \tag{20}$$

where

$$B = \sqrt{\frac{2\kappa}{R(\kappa - 1)}} \tag{21}$$

$$\Pi = \left(\frac{2}{\kappa + 1}\right)^{\frac{1}{\kappa - 1}} \sqrt{\frac{\kappa}{R(\kappa + 1)}} \tag{22}$$

The dimensionless dynamic equation can be written as follows.

$$\frac{d^2\theta}{d(t^*)^2} = \frac{1}{t_f^{*2}}\left[\frac{1}{2}\left(p_1^* - p_2^*\right) G_a(\theta) - \left(\frac{1}{t_{c1}^*}\right)^2 \ldots\right] - 2\varepsilon\, G(\theta)\, G'(\theta)\left(\frac{d\theta}{dt^*}\right)^2 - \varepsilon\, G(\theta)^2 \frac{d^2\theta}{d(t^*)^2} \tag{23}$$

where, the dimensionless parameter t_f^* which is the dimensionless inertia parameter is can be expressed as follows.

$$t_f^* = \frac{t_f}{t_b} \tag{24}$$

$$t_f = \sqrt{\frac{J L_b}{p_s A_b}} \tag{25}$$

The parameter ε is the ratio of reciprocating inertia and moment of inertia, which can be written as follows

$$\varepsilon = \frac{Mr^2}{J} \tag{26}$$

The dimensionless parameters about load can be given by

$$t_{c1}^* = \frac{\sqrt{J/c_1}}{t_b} \tag{27}$$

$$t_{c2}^* = \frac{J/c_2}{t_b} \tag{28}$$

The dimensionless equation of movement can be given as the following equations

$$y^* = \frac{1}{2} + \frac{1}{2}\left(\ldots - \cos\theta\right) \tag{29}$$

$$V k y^{**} = + {}_{d} \quad (30)$$

$$\frac{dV^*}{dt^*} = 2M \Gamma^{*22} \text{(OMOON)} / 1 \sin\sin \sqrt{} \quad (31)$$

$$A_w^* = 24 \frac{y^*}{D^*} \quad (32)$$

The dimensionless state equation can be expressed as:

$$p V m R T^{****} \quad (33)$$

SIMULATION AND ANALYSIS

The performance analyses of CAE can be divided into two parts. One is energy efficiency which is useful in the design, optimization and evaluation of CAE system. The other is output power which is an important factor in the application of a CAE.

Dimensionless energy efficiency can be expressed as

$$\Gamma^* = \frac{W^*}{E^*} \quad (34)$$

where

$$W p d V^{***} \quad (35)$$

$$E m T^{***}_{in} \ln \frac{\varphi \ \ k}{\phi \ p_a^*} \quad (36)$$

Dimensionless output power can be expressed as

$$p_{me}^* = \frac{T^{**} W}{2M} \quad (37)$$

From the discussion above, it can be found that the dimensionless energy efficiency and output power of the CAE is determined by fourteen dimensionless parameters. Because load is diverse and complex, the dimensionless parameters about load are considered constant value. Therefore, the influencing parameters become twelve dimensionless parameters. The initial values of the fourteen dimensionless parameters are shown in Table 2. The software, MATLAB/SIMULINK, is used for modeling the simulation. Figure (6) depicts the speed characteristics, efficiency characteristics and output power characteristics of the CAE.

Table2. The initial values of the parameters

Parameter	t_{hc}^*	D^*	λ	T_1^*	p_2^*	k_d
Value	1	0.2	0.314	1	0.1	0.1
Parameter	τ_1	τ_2	θ_1^*	θ_2^*	t_f^*	ε
Value	0.5	0.5	pi/3	2pi	0.6	0.01

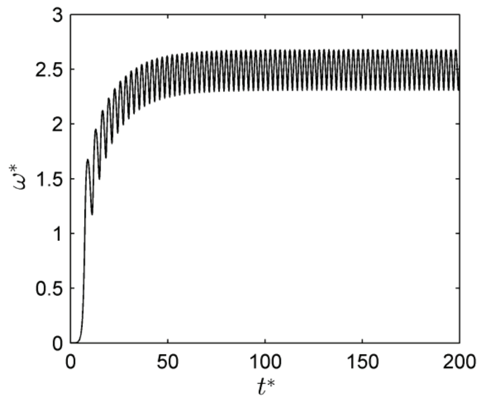

(a)

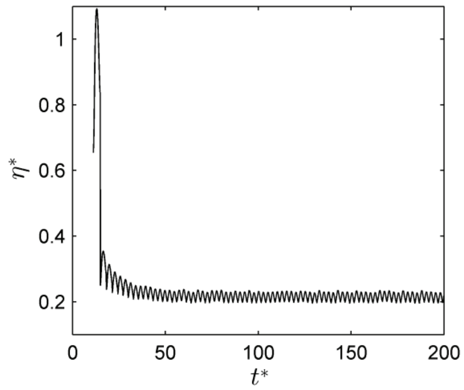

(b)

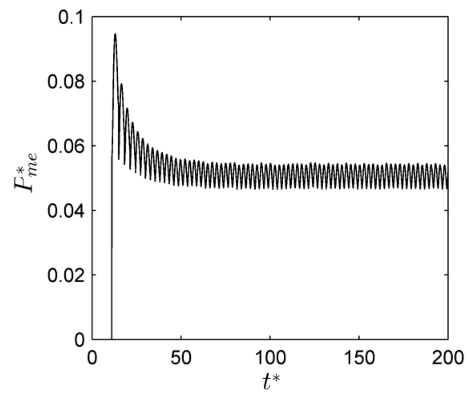

(c)

Figure 6 Dimensionless speed, dimensionless efficiency and dimensionless output power curves

Figure 6(a) shows the dimensionless speed curves during the starting process. About the dimensionless time is about 50-60, the dimensionless speed tends to stabilize, but the fluctuation is quiet apparent.

Figure 6(b) shows the dimensionless efficiency curves during the starting process. It is obvious that the dimensionless efficiency decreases with dimensionless speed increasing.

Figure 6(c) shows the dimensionless output power curves during the starting process. It is obvious that dimensionless output power fluctuation is quiet apparent in stable phase.

Dimensionless Efficiency Analysis

According to the dimensionless model above, each dimensionless parameter can be changed for comparison while all other dimensionless parameters are kept constant.

The change rate of the dimensionless efficiency is the ratio of the change in the dimensionless efficiency for one parameter and the total change in the dimensionless efficiency for all parameters.

Figure (7) describes the rate of change of the dimensionless efficiency for each parameter

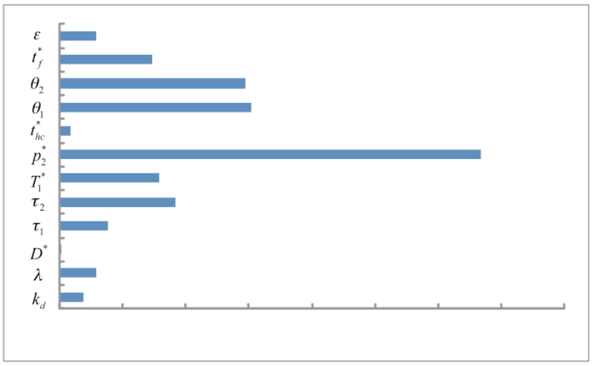

Figure 7 Rate of change of efficiency for each parameter

It can be seen form Figure (7) that:

(a) The dimensionless efficiency is impacted significantly by the dimensionless exhaust pressure, intake duration angle, and exhaust duration angle. The rates of change of the efficiency for the three parameters are 0.3343, 0.1522 and 0.1471.

(b) The dimensionless efficiency is slightly affected by the dimensionless inertial moment parameter, the scale factor of exhaust valve, the dimensionless intake temperature and the scale factor of intake valve.

(c) There is little influence of the dimensionless temperature settling time, the dimensionless cylinder diameter, the ratio of crank radius and connecting rod length, the ratio of cylinder clearance and exhaust volume, and the ratio of reciprocating inertia and moment of inertia.

Dimensionless Power Analysis

The change rate of the dimensionless power is the ratio of the change in the dimensionless power for one parameter and the total change in the dimensionless power for all parameters.

Figure (8) describes the rate of change of the dimensionless power for each parameter

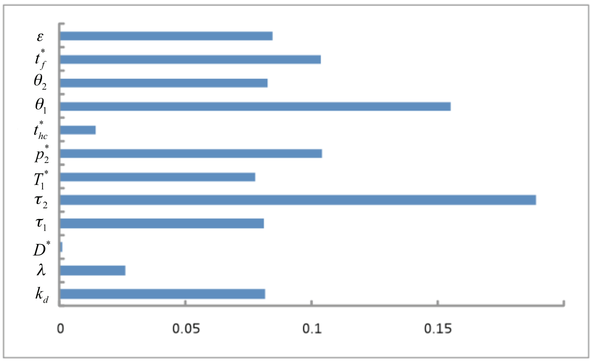

Figure 8 Rate of change of power for each parameter

It can be seen form Figure (8) that:

(a) The dimensionless power is impacted significantly by the scale factor of exhaust valve, intake duration angle, the dimensionless exhaust pressure and the dimensionless inertial moment parameter. The rates of change of the power for the four parameters are 0.189, 0.1551, 0.1042 and 0.1036, respectively.

(b) The dimensionless power is slightly affected by the scale factor of intake valve, exhaust duration angle, the ratio of reciprocating inertia and moment of inertia, the ratio of cylinder clearance and exhaust volume, and the dimensionless intake temperature.

(c) There is little influence of the dimensionless temperature settling time, the dimensionless cylinder diameter, the ratio of crank radius and connecting rod length.

THE OPTIMAL DESIGN OF CAE

Structural parameters optimization

The CAE's performance indicators include power output P_{me}, working efficiency η. These indicators can be calculated by following expressions:

$$\begin{cases} P_{me} = pW/t \\ \eta = P_{me} / \left(m R T_1 \ln(p_s/p_a) \right) \end{cases} \qquad (38)$$

Structural parameters of the engine cannot be changed easily, in addition, simulation analysis shows the intake pressure and the distribution parameters including intake duration angle, exhaust duration angle and the scale factor of exhaust valve are key factors that influence the CAE performances.

There, intake and exhaust process are controlled by a five polynomial cam curve which is chosen as follows [26].

$$h(x)=C_0+C_px^p+C_qx^q+C_rx^r+C_sx^s \tag{39}$$

In there, p=2, q=2n, r=2n+2m, s=2n+4m.

Other coefficient can be solved by boundary conditions which can be expressed by following expressions:

$$\begin{cases} C_p=\dfrac{2C_0 qrs}{(q-p)(r-p)(s-p)} \\ C_q=\dfrac{2C_0 prs}{(p-q)(r-q)(s-q)} \\ C_r=\dfrac{2C_0 pqs}{(p-r)(q-r)(s-r)} \\ C_s=\dfrac{2C_0 pqr}{(p-s)(q-s)(r-s)} \end{cases} \tag{40}$$

where v is seating velocity.

To meet certain performances, some structure specifications of the single-cylinder parameters are shown in table3.

Table3. Engine main Specifications

Type	Specification
Number of cylinder	1
Bore x Stroke	85.0mm×88.0mm
Displacement Cylinder dead volume(m^3)	499cc 0.4×10^5
Crank-Link Rod Ratio	0.316
Supply pressure (MPa)	2
Engine speed(w)	1000rpm
Intake port diameter(IPD)	12mm
Exhaust port diameter(EPD) Intake valve rod diameter(d_{1in}) Exhaust valve rod diameter(d_{1out})	12mm 7mm 7mm

According to study in the literature [27-28] and the size of the engine structure, ranges of the parameters are shown in Table 4.

Table 4. Range of the parameters

IVL/(°)	θ_1/(°)	CVL/(°)	θ_2/(°)
2~7	20~90	2~7	346~356
m_{intake}	n_{intake}	$m_{exhaust}$	$n_{exhaust}$
1~10	3~20	1~10	3~20

The independent analysis of individual parameters shows that different indicators of the CAE cannot achieve optimum at the same time. In conclusion, the design of the CAE is a multi-parameter and multi-objective optimization problem. The coupling of the parameters should be considered and an effective comprehensive evaluation method is indispensable.

In this paper, orthogonal design [29] was carried out to cover the discrete combinations of different parameters. The optimal parameter combination for the expected indicators was obtained using grey relation analysis [30-31].

In the following, GRA method was used to solve the optimal design of CAE problems.

Step1.Based on the orthogonal array method, parameter combinations were obtained.

Step 2. Calculate the decision matrix D_{ij}

D_{ij} is the calculated value of the evaluation set which is formed by the indicators in equations (38). i is No.i parameter combination, and j is indicator number. And then $D=(D_{ij})_{N\times2}$ is decision matrix.

Step3. Given the range of expected indicators

The vector of expected indicators is expressed as $D_{0min}=(D_{01min},D_{02min})$ and $D_{0max}=(D_{01max},D_{02max})$ whose value is set according to design requirements.

Step 4. Dimension of decision matrix

Decision matrix can be made dimensionless matrix by using the range of expected indicators, which can be expressed by following equation:

$$f(D_{ij})=\begin{cases} 0 & D_{ij}\le D_{0min} \\ \dfrac{(D_{ij}-D_{0min})^2}{(D_{0max}-D_{0min})^2} & D_{0min}<D_{ij}\le D_{0max} \\ 1 & D_{ij}>D_{0max} \end{cases} \tag{41}$$

Step5. Calculated the relational degree

The relational degree between the calculated indicators of corresponding parameter combination and the expected indicators can be calculated by:

$$R_i=\sum_{j=1}^{2}W_j f(D_{ij}) \qquad i=1,2,...,N \tag{42}$$

where W_j is the vector of weight, in the paper, $W_j=(0.5,0.5)^T$.

The optimal parameter combination can be determined by the value of R_i, The bigger R_i is, the more the calculated indicators are fit with the expected maximum indicators. In addition, the optimal indicators and parameter combination can be obtained.

Through simulating calculations, the optimal performance indicators and corresponding combination of parameters within the ranges are obtained and shown in Table 5 and Table 6.

Table 5 the range of performance indicators and optimal performance indicators

Performance indicator	Range value	Optimal value
P_{me}(kW)	1~2	2.027
η(%)	35~50	50.13

Table 6 Optimal combination of the parameters

IVL/(°)	θ_1/(°)	CVL/(°)	θ_2/(°)
3.2	70	5.7	348
m_{intake}	n_{intake}	$m_{exhaust}$	$n_{exhaust}$
3	6	3	6

Operating parameter optimization

In the real operations, the performance of the engine needs to be adjusted to cope with demands of the loading system. To achieve a given output power and high energy efficiency, the intake pressure and ratio of transmission can be optimized, which is a typical multi-objective engineering optimization.

The genetic algorithm (GA) is a powerful, general-purpose optimization tool, widely used to solve optimizing problems in the mathematics, engineering and so on. Genetic algorithm works with a population of feasible solutions; therefore, it can be used in multi-objective optimization problems to obtain a number of solutions simultaneously. NSGA-II, proposed by Devetal, is a fast and elitist multi-objective GA [32]. The crossover and mutation operators remain as usual, but selection operator works differently from simple GA. Selection is done with the help of crowded-comparison operator, based on ranking (according to non-domination level), and crowding distance. The crowding distance is briefly explained below [33].

To guarantee a good diversity of the individual point, the following questions must be solved.

(1)The threshold value about adjacent individual must be defined.

(2)Which individual is selected when adjacent individual distance is less than the threshold value?

Firstly, the minimum and the maximum extreme endpoint are found in current elitist sorting. Then the distance of the two extreme end points are calculated which indicated by $d_{\max}$. The threshold value can be written by:

$$\int = \frac{d_{\max}}{2 \notin num} \tag{43}$$

where, *num* is the number of individual.

The threshold individual selection can be shown in Figure (9).

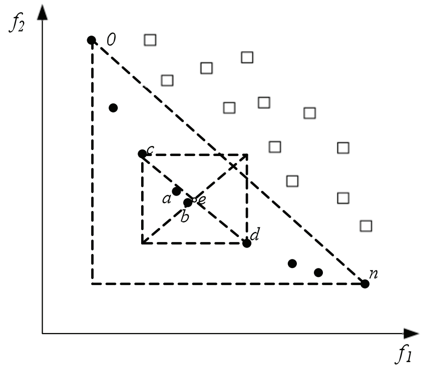

Figure9. The crowding distance calculation and individual selection

As shown in Figure (9), if the Euclidian distance between the individual *a* or *b* is less than or equal to the threshold value, adjacent individual *c* and *d* are found, and the center point *e*, between *c* and *d*, can be obtained. If the distance between *a* and *e* is less than *e* and *b*, the individual *b* is deleted.

In the present study, the range of the intake pressure is between 1MPa and 3MPa, the range of ratio of transmission is between 0.4 and 1.2.

The non-dominated solution set, obtained over the entire optimization procedure, are shown in Figure 10.

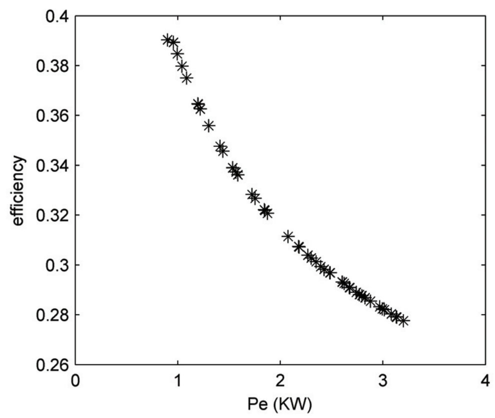

Figure10. Improved NSGA-II Pareto-optimal set

PRESSURE COMPENSATED VALVE

To prevent air leakage, the spring preload should be greater than the inertia force of the valve, which is decided by a certain safety factor. A stronger spring was designed by Chih-yuang et al. [19] to increase the preload. However, the increased spring pre-loading causes the valve actuator to consume more energy. This paper describes pressure compensated valve which refers to Sasa Trajkovic, et al. [34] in order to make it possible to achieve desired closing and opening at high pressure.

The pressure-compensated intake valve is shown in Figure (11). The pressure-compensated mechanism was applied in the valve stem. The O-ring rubber seal prevents leakage while the valve stem moves. The valve spring is installed on the cylinder head, which can ensure that the valve opens and closes.

The pressurized air enters the air passages on the intake valve and is guided up to the pneumatic valve spring. Since the compressed air in the air passage acts on the intake valve, as indicated by the red arrows, the net force should be zero, and thus the valve should be pressure compensated. This means that the cylinder will be kept closed without using any valve spring and the valve diameter can now be increased in order to reduce the pressure drop. The intake valve and exhaust valve were designed as Figure (12).

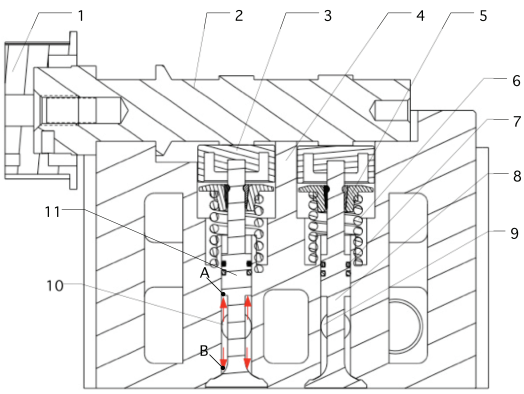

1 pulley wheel 2 camshaft 3 top cup 4 cylinder head 5 valve split collet 6 preload spring 7 O-ring rubber seal 8 exhaust valve 9 exhaust port 10 intake port 11 the intake valve

Figure 11 A simple cross section illustration of the cylinder head

Figure12. The photo of intake valve

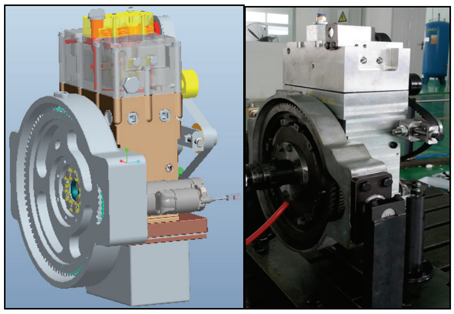

Figure13. Physical model and photo of the CAE

Based on optimal structure parameters and pressure compensated valve, prototype of CAE is designed referring to internal combustion engine. Figure (13) shows the CAE model and photo.

TEMPERATURE DROP ANALYSIS AND HEAT EXCHANGE SYSTEM DESIGN

To predict temperature drops, prevent the ice blocking problem and improve the performance of the CAE system during the operation, the thermodynamic model of the CAE and a calculation method for equivalent air temperatures at intake and exhaust ports are described.

Serving as the engine of vehicles, the practical CAE has its inlet pressure higher than 1MPa so that it can output enough power. And sufficient compressed air is needed to meet the demand of a certain mileage. Thus the practical CAE system's air source is a high pressure system, as shown in Figure (14). Besides the high pressure tanks group, in order to stabilize the intake flow, a low pressure buffer tank and a reducer is added before the inlet of the CAE. A dynamic system model was built according to the principle in Figure (15). Air pipes before the high pressure reducer and after the low pressure reducer are ignored because they are relatively short, then the pipelines in the system model are simplified as one pipe model between the high pressure reducer and the buffer tank.

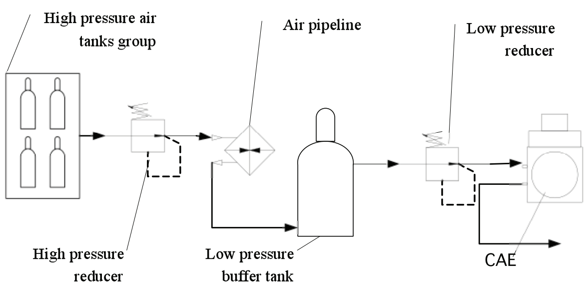

Figure14. Schematic diagram of a practical CAE system

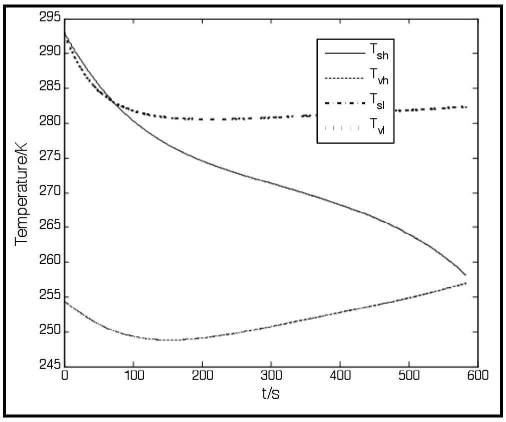

Figure15. Curves of T_{sh}, T_{vh} T_{sl} and T_{vl} during the running process of the dynamic model.

In the simulation process, the room temperature was set as 293K. Thus, temperatures of all inner walls in the system model were ideally assumed to be equal to 293K. The CAE model was running until the pressure in the buffer tank was lower than 5MPa. In the case of rotate speed 1000rpm, the engine's output power reaches 5kW. During the operation, air temperatures in the high pressure tank (T_{sh}), at the export of the high pressure reducer (T_{vh}), at the export of the buffer tank (T_{sl}) and at the export of the low pressure reducer (T_{vl}) were monitored and are shown in Figure (15).

As can be seen, T_{sh} drops dramatically, at the end of the operation its lowest value reaches 258K. Due to the large pressure difference, the instant temperature drop after the reducer is severe, especially in the initial stage of the operation. Though the temperature recovers slowly after 150s, the highest value of T_{vh} is lower than 257K. Sustained low temperature makes the reducer's outlet very easy to have ice blocking. Heat exchanges with the pipeline and the buffer tank is effective so that T_{sl} is higher than 280K at most of the time. But after the throttling of the low pressure reducer, T_{vl} which is equal to the inlet temperature drops to lower than 270K. At about 300s, the inlet air temperature is 265.8K. The calculated equivalent air temperatures at intake and exhaust ports of the CAE are 268.8K and 225.6K respectively. It shows the very bad temperature condition at the exhaust port.

A heat transfer system for the practical CAE system is designed with its structure diagram shown in Figure (16). On the basis of the original system shown in Figure (14), a set of heat exchange pipe (4) with total length 4m and diameter 0.006m is added between the tanks group (1) and the high pressure reducer (11). Size of the pipe after the reducer (10) is changed into the same size as pipe (4). Positions of the buffer tank (8) and the low pressure reducer (7) are swapped. This measure can make the temperature difference between the inlet air and the inner wall of the buffer tank (8) bigger, resulting in better heat transfer effect in the tank. Then the modified model was simulated. Air temperature curves in the high pressure tanks (1) (T_{sh}), at the export of the pipe (4) (T_{ph}), at the export of the pipe (10) (T_{pl}) and at the export of the buffer tank (8) (T_{sl}) are shown in Figure (15). As can be seen, these improvements can make the air temperature in the supply pipelines (2) more close to the room temperature. When all the temperatures are higher than 273K, no ice block will happen before the inlet of the CAE. When the inlet air temperature is about 282K, the equivalent temperatures at intake and exhaust ports raise to 285K and 230K respectively.

For piston-type engine, the intake and exhaust system located on the cylinder head (9), thus a heat exchange chamber is placed in the cylinder head (9) so that a heat transfer medium can flow in it to prevent excessive cooling. The heat transfer medium is stored in an engine radiator assembly (13) which is composed of a radiator tank and a fan. The medium of low temperature absorbs heat from the atmosphere through the radiator and the temperature rises. Then the liquid is extracted by a pump (5) out of the tank. Through the medium pipelines (3), it flows through the cylinder head (9), heat exchange pipes (4), (10) and returns to the radiator tank (13).

In addition, the high pressure reducer is a major cause of energy loses in the pneumatic system. In the simulation of the high pressure CAE system, the average air flow through the reducer is 0.0425kg/s. The pneumatic power loses due to the reducing process is approximately 6.3kW which is even higher than output power of the CAE. Therefore the high pressure reducer is modified into a pressure reducing and energy recovery device (11). It is functionally combined by a high pressure rotary motor and a reducer. When the CAE is not running, it plays the role of a pressure reducer. When there is mass flow in the pipeline, part of the energy can be recycled by the rotary motor to drive the pump (5) and the radiator fan (13) through transmissions (6) and (12). Thus the heat exchange system can be running automatically during operation of the engine without additional energy consumption.

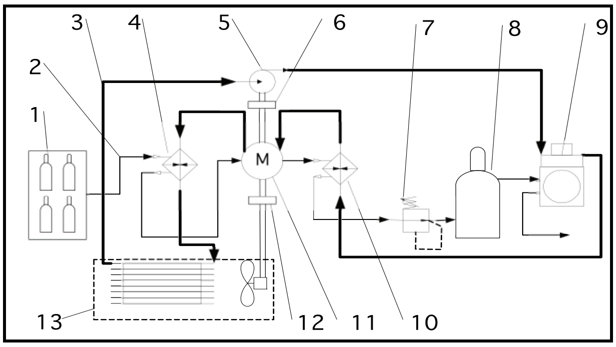

1.Tanks group 2.Supply pipeline 3.Medium pipeline 4,10.Heat exchange pipe 5.Pump 6,12.Transmissions 7.Low pressure reducer 8.Buffer tank 9.Cylinder head 11.Energy recovery device 13.Radiator assembly

Figure 16**.** Structure diagram of the heat exchange system for the CAE system.

EXPERIMENTAL INVESTIGATION

Experimental setup

In this study, the CAE was designed based on the CAE working characteristics. The engine was modified and connected to a compressed air tank. The intake port of the engine was connected to a compressed-air supply system that contained a 10bar air compressor (US11-10, Screw air compressor, United OSD, Germany). The pressure regulator adjusted the compressed-air pressure to the requirements of various experiments. The test bench includes an eddy current dynamometer (DWZ6, rated torque 25 Nm, maximum speed 12000rpm, CHENGBANG, Sichuan, China) to measure the power output and the speed of the test engine. The electromagnetic brake produces a load that varies from 0 to 25Nm. Two pressure transducers (JYB-KO-MAG1, ColliHigh) and two thermocouples were installed at the inlet and the exit of the engine to monitor the pressure and the temperature during the test. To record the cylinder pressure during the experiments, the KISTLER pressure sensor (4075A) was used to measure the absolute pressure. A gas turbine flow meter (LWQ-A/20(FL), Tianjin Sure Instrument Science & Technology Co. LTD, China) was installed at the engine inlet to record the flow rates. An absolute rotary encoder acquired the piston location in the cylinder during the engine operation. All data acquired from the experiments were transferred to a data acquisition unit for recording and further analysis. Figure (17) shows the schematic of the compressed-air engine test bench and picture of the experimental test bench.

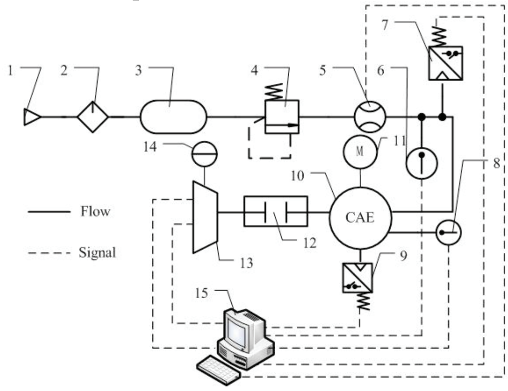

1.Compressor	9.High precision pressure sensor
2.Water filter	10.Engine
3.Buffer tank	11. Starter
4.Pressure regulator	12.Coupling
5.Flow meter	13.Eddy current dynamometer
6.Inlet thermocouple	14.Power supply
7.Inlet pressure sensor	15.Data acquisition system
8.Outlet thermocouple	

Figure17. The CAE loop test and its test bench

Results and analyses

When the intake pressure is adjusted form 0.25MPa to 0.45MPa, the output power and torque are measured in different rotate speed. The results are shown in Figure (18).

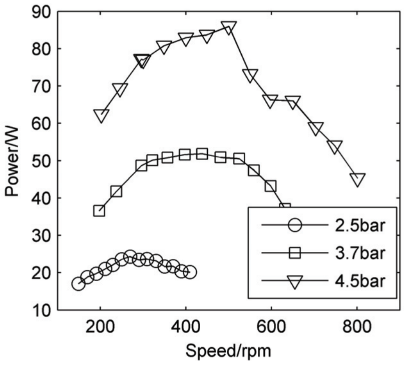

(*a*)

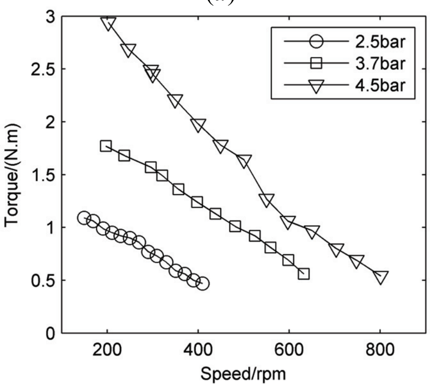

(*b*)

Figure18. Output power and torque at different speeds and supply pressure

The highest output power is obtained at the highest supply pressure and 500rpm speed. It is obvious that the optimal speed can be obtained in different intake pressure. And the highest torque is obtained at the highest supply pressure and lowest speed.

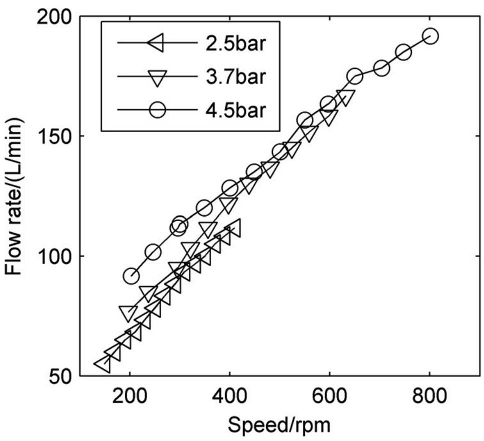

Figure 19 Flow rate at different speeds and supply pressure

The volume flow rate is measured in different rotate speed. The results are shown in Figure (19). It is obvious that the volume flow increases with the supply pressure and speed increasing.

To verify the mathematical model for single-cylinder CAE, the intake pressure and the rotate speed were set to 0.45MPa and 402rpm, respectively. The cylinder pressure data was obtained by the simulation and KISTLER pressure sensor with crank angle as shown in Figure (20).

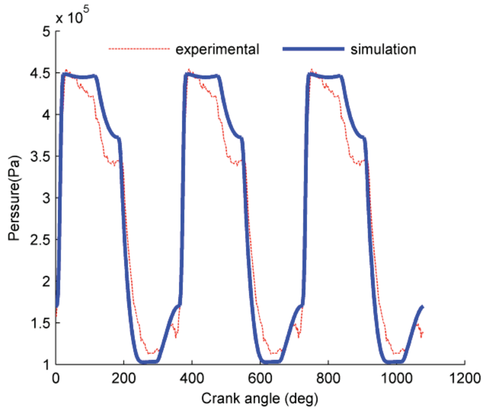

Figure20. Fluctuation of the cylinder pressure

As shown in Figure (20), the simulation results are clearly consistent with the experimental results, which verify the described mathematical model. However, there are three differences between the simulation results and the experimental results:

(a) The experiment results have a lower cylinder pressure than the simulation results during the expansion process.

(b) The experiment results have higher cylinder pressure than the simulation results during the exhaust process.

(c) The cylinder pressure will decrease when the intake valve is opened during the experiment.

The main reasons for the differences are summarized as follows.

(a) There is a gap between the piston seal ring and the cylinder, the compressed air in the cylinder will leak out during the CAE working process. When the intake valve and the exhaust valve are closed, the cylinder pressure decreases. However, the simulation is based on the assumption that there is no leakage in the working process.

(b) The actual critical pressure ratio depends on the shape of the flow path in the device; the ratio will deviate from 0.528. However, the simulation is based on the assumption that the critical pressure ratio is 0.528.

(c) When the piston reaches to the top dead center (TDC), the intake valve was not opened. So when the piston moves to the bottom dead center (BDC), the cylinder volume will increase which lead to cylinder pressure decrease.

Other uncontrollable factors in the experiment, such as the fluctuation of the supply pressure, the heat exchange and the atmospheric temperature, also influence these differences between the simulation and the experimental results.

CONCLUSIONS

In this paper, the working process of the CAE was studied. Based on the basic mathematical model in the authors' previous study, appropriate reference values were selected, the basic mathematical model was transferred to a dimensionless expression, the energy efficiency and output power was analyzed through simulation. To obtain good performance, the main influence parameters were optimized by grey relation analysis. Then to prevent the ice blocking problem during the operation, temperature drop was analyzed and heat exchange system was designed. At last, the CAE performance was investigated by experiment. The conclusions are summarized as follows:

(1) The simulation results are clearly consistent with the experimental results, which verify the described mathematical model.
(2) The dimensionless efficiency is impacted significantly by the dimensionless exhaust pressure, intake duration angle, and exhaust duration angle.
(3) The dimensionless power is impacted significantly by the scale factor of exhaust valve, intake duration angle, the dimensionless exhaust pressure and the dimensionless inertial moment parameter.
(4) The optimal output power and efficiency values are 2.027kW and 50.13%, respectively.
(5) Simulation results show that the heat exchange system can maintain the air temperatures in the supply system above 0 ℃, preventing the ice blocking problem before the inlet of the APE. In addition, the energy loss due to the high pressure reducing process can be used to drive the heat exchange system.

The analyses of this paper can provide a theoretical basis for the design of CAE system.

References

1. Shahriar Shafiee , ErkanTopal., When will fossil fuel reserves be diminished? Energy policy, 2009; 37(1), pp.181-189.
2. Pierre Gadonneix, Abubakar Sambo, et al. World Energy Resources 2013 Survey.
3. Sheu KB and Hsu TH, Design and implementation of a novel hybrid-electric-motorcycle transmission, Apply Energy, 2006, 86, pp.859-74.
4. Sheu KB, Analysis and evaluation of hybrid scooter transmission systems. Apply Energy, 2007, 84, pp.1289-304.
5. Huang KD, Tzeng SC, Chang WC, Development of a hybrid pneumatic-power vehicle. Apply Energy, 2005, 80, pp.47-59.
6. Huang KD, Tzeng SC, A new parallel-type hybrid electric-vehicle. Apply Energy, 2004, 79, pp.51-64.
7. V. Motevalli, New approach for performing failure analysis of fuel cell powered vehicles. International Journal of automotive technology, 2009, 06, pp.743-752.
8. Karabasoglu, O., Michalek, J., Influence of driving patterns on life cycle cost and emissions of hybrid and plug-in electric vehicle powertrains. Energy Policy, 2013, 60(1), pp.445-461.
9. Afzal Ahmed, A pilot compressed air engine. Energy and Environment, 2011, 22(8), pp.1105-1113
10. JP Yadav and Bharat Raj Singh, Study and Fabrication of Compressed air Engine, S-JPSET , 2011, 2(1), pp.1-8.
11. Kato, Yuki, Hayashi, A. Koichi, Yamada, Eisuke, Study on development of compressed air car for a practical use. FISITA2010-SC-P-05.
12. Yu-Ta Shen, Yean-Ren Hwang, Design and implementation of an air-powered motorcycles, Applied Energy, 2009, 86, pp.1105-1110.
13. Zhang Y, Nishi A, Low-pressure air motor for wall-climbing robot actuation, Mechatronics, 2003, 13, pp.377-92.
14. J.F. Gairns (1904). Industrial locomotives for mining, factory, and allied uses.Part II.- compressed air and internal combustion locomotives. Cassier's Magazine16: 363-377.
15. http://www.engineair.com.au/
16. Zhai X, Research on hybrid of compressed-air and fuel. PhD Thesis, Zhejiang University, China, 2005.
17. Felix Creutzig, Andrew Papson, Lee Schipper and Daniel M Kammen, Economic and environmental evaluation of compressed-air cars, Environ. Res. Lett, 2009,4(044011), pp.1-9.
18. Lin LIU, Xiaoli Yu, Practicality study on air-powered vehicle, Front. Energy Power Eng. China 2008, 2(1), pp.14-19.
19. Huang CY, Hu CK, Yu CJ, et al. Experimental investigation on the performance of a compressed-air driven piston engine, Energies, 2013, 6, pp.1731-1745.
20. Wang Y, Liu XY, Zhou Y. Design and performance analysis of a triangle rotary piston air-powered engine. Mechanical Science and Technology for Aerospace Engineering 2009; 28: 950-954.
21. Nie XH, Yu XL, Hu JQ, et al. Influence of inlet and outlet valve's open timing on pneumatic engine and their optimal design. Journal of Engineering Design 2009; 16: 16-20.
22. Xu QY, Cai ML, Yu QH, et al. Multi-parameter and multi-objective optimization method for air

powered engine. Journal of Beijing University of Aeronautics and Astronautics 2013; 39: 803-807.
23. Liu H. Research on air powered vehicle engine. PhD Thesis, Zhejiang University, China, 2004.
24. Qihui Yu, Maolin Cai , Yan Shi, Zichuan Fan, Optimization of the energy efficiency of a piston compressed air engine. Strojniški vestnik-Journal of Mechanical Engineering, 2014, 60(6), pp.395-406.
25. Kagawa, T, Heat Transfer Effects on the Frequency Response of a Pneumatic Nozzle Flapper, ASME J. Dyn. Sys. Meas. Control, 1985, 107(4), pp.332-336.
26. Junzhen He, Xuefeng Li, Optimization Design of the Cam profile of a High-order Polynomial Using MATLAB, Mechanical Science and Technology for Aerospace Engineering, 2008, 27.
27. Yu QH , Shi Y, Song Rz, et al. Dimensionless study on outlet torque characters. J Beijing Univ Aeronaut Astronaut, 2013, 39(9), pp.1233-1237.
28. Xu QY, Cai ML, Yu QH, et al. Multi-parameter and multi-objective optimization method for air powered engine. J Beijing Univ Aeronaut Astronaut, 2013, 39(6), pp.803-807.
29. Chen JL, Au KC, Wong YS, et al. Using orthogonal design to determine optimal conditions for biodegradation of phenanthrene in mangrove sediment slurry, J Hazard Mater, 2010, 176, pp.666-671.
30. Xia XT, Li JH, Influence of vacuum on friction torque of rolling bearing for space applications based on optimum grey relational space. J grey syst , 2011, 23, pp.327-334.
31. Wei GW, GRA method for multiple attribute decision making with incomplete weight information in intuitionistic fuzzy setting, Knowl Based Syst ,2010, 23, pp.243-247.
32. Kalyanmoy Deb. A Fast and Elitist Multi-objective Genetic Algorithm: NSGA-II. Transactions on evolutionary computation, 2002, 6(2), pp. 182-197.
33. Debabrata Mandal, SurjyaK.Pal, ParthaSaha. Modeling of electrical discharge matching process using back propagation neural network and multi-objective optimization using non-dominating sorting genetic algorithm-II. Energy Conversion and Management , 2007 , 48 , pp.1029-1041.
34. Sasa Trajkovic, Per Tunesta, Bengt Johansson. Investigation of different valve geometries and valve timing Strategies and their effect on regenerative efficiency for a pneumatic hybrid with variable valve actuation. SAE Paper 2008-01-1715.